This article has been accepted for publication in a future issue of this journal, but has not been fully edited. Content may change prior to final publication. Citation information: DOI 10.1109/TPEL.2018.2889107, IEEE Transactions on Power Electronics

A Power Electronic Traction Transformer Configuration with Low-Voltage IGBTs for Onboard Traction Application

Jiepin Zhang, *Student Member*, *IEEE*, Jianqiang Liu, *Senior Member*, *IEEE*, Shigeng Zhong, Jingxi Yang, *Student Member*, *IEEE*, Nan Zhao, *Student Member*, *IEEE* and Trillion Q. Zheng, *Senior Member*, *IEEE*

***Abstract*—Solid-state transformer (SST) for onboard traction application is also addressed as power electronic traction transformer (PETT), which is used to replace the line frequency traction transformer (LFTT) and four-quadrant converter (4QC) to further improve efficiency, save installation space, and reduce weight of the onboard equipment. However, based on the conventional PETT configuration with the modular series-parallel structure, it is hard to guarantee the high efficiency and high power density at the same time due to the limitations caused by the switching characteristics of the semiconductor devices, transformer design, and high-voltage insulation design, etc. To deal with the mentioned problem, a PETT configuration and the parameters' design method for onboard traction application are proposed in this paper to replace the conventional dc/dc stage with the low-voltage IGBTs. By using the proposed configuration, the high-voltage IGBTs can be replaced by the low-voltage IGBTs, which can help reduce switching loss. Meanwhile, zero-current switching (ZCS) or zero-voltage switching (ZVS) for all the IGBTs can be guaranteed, and the number of the medium-frequency transformers (MFTs) will not increase. Therefore, a multiple optimization of PETT, including switching losses, the number of MFTs and switches, and costs, can be finally achieved. Finally, an experimental prototype is built to verify the performance of the proposed PETT configuration.**

***Index Terms*—Solid-state transformer (SST), power electronic traction transformer (PETT), traction, control strategy, parameters design, efficiency, power density, costs, insulation.**

I. Introduction

POWER electronic transformer (PET) is a kind of power electronic converter with the characteristics of high frequency, bidirectional power flow, and electrical isolation, which is also known as solid-state transformer (SST), energy router, smart transformer, etc. The concept of PET has been studied for several decades, which contains two major motivations in general. One is to improve power control performance and achieve interconnection, such as for the distribution grid [1]-[3], DC microgrid [4]-[5], etc. Another one is to improve efficiency, reduce volume and weight, such as for the onboard traction system [6]-[8], nacelles of wind turbines [9], future electric aircrafts, and ships [10]-[11], etc. About the second motivation, the most prominent and urgent application is the onboard traction system. For the onboard traction system, almost 33% of the weight of the electric equipment is occupied by the onboard line frequency traction transformer (LFTT). Thus it is significant to make LFTT smaller and lighter. Moreover, reducing weight and volume of LFTT can help save energy, improve running speed, and increase available space for passengers or cargos. It can also reduce the pressure between the train and rail. Recently, many energy-storing devices, such as fuel cells, super-capacitors, and lithium batteries, have been installed and tested in the urban railway vehicles and high-speed trains. In this case, reducing the weight and volume of the previous electric equipment become more and more important. Furthermore, since the allowable weight and volume of a traction transformer is limited, LFTTs tend to be quite inefficient (typically around 90 % [12]), which further creates the motivation for the application of PET.

PET in the onboard traction system is usually addressed as power electronic traction transformer (PETT) [6]. In recent years, many famous railway traction system suppliers and research institutions have been making a study of PETT, such as ABB, Alstom, Bombardier, Siemens, etc. Moreover, various topologies were proposed and the corresponding prototypes were built. In 2003, a 1.5 MVA prototype with 8-module cascaded H-bridge (CHB) plus multi-winding resonant DC/DC converter was built by Alstom, and the switching frequency of the isolated DC/DC stage is 5 kHz [13]. In [14], a 2MVA, 8-module 17-level MMC topology is proposed by Siemens, whose switching frequency is only 1 kHz hence of the hard switching. Then a 1.2MVA, 16-module cascaded matrix converter is proposed by ABB in 2007 [15]. Though the DC/DC stage is canceled, the switching frequency is just 400 Hz and the structure is complex. After that, the CHB-based modular series-parallel configuration (CHB plus isolated DC/DC converter) becomes more popular and mature [8], whose typical configuration is shown in Fig. 1 and is called configuration 1 in this paper. In 2007, a 750 kW lab test system with 8-module CHB plus LLC resonant converter is proposed by Bombardier [16]. The switching frequency in DC/DC stage can reach to 8 kHz. In 2011, a 1.2 MVA PETT prototype with 9-module CHB plus LLC resonant converter for a 15 kV/16.7 Hz railway grid is developed by ABB, which has been installed on a test locomotive and the efficiency is around 96%. It is also the first PETT prototype to be commissioned and installed on a shunting locomotive [6], [7], [17]-[19]. However, in this PETT prototype, the frequency of the isolated dc-dc link is only 1.75 kHz. According to the above results provided by these companies, high-voltage IGBTs (6.5kV or 3.3kV) are usually used to reduce the number of the modules. However, since the poor switching characteristics of the high voltage IGBTs, the

This work was supported by National Key R&D Program of China under Grant 2017YFB1200900, and by the CRRC Corporation, Ltd.

The corresponding author is Jianqiang Liu. All of the authors are with the Institute of Power Electronics and Electric Traction, Beijing Jiaotong University, Beijing China, 10044. (E-mail: jiepinzhang@bjtu.edu.cn, liujianqiang@bjtu.edu.cn, 17121545@bjtu.edu.cn, yangjingxi@bjtu.edu.cn, zhaonan@bjtu.edu.cn, tqzheng@bjtu.edu.cn.)

This article has been accepted for publication in a future issue of this journal, but has not been fully edited. Content may change prior to final publication. Citation information: DOI 10.1109/TPEL.2018.2889107, IEEE Transactions on Power Electronics

switching frequency cannot be efficiently increased (usually lower than 5 kHz).

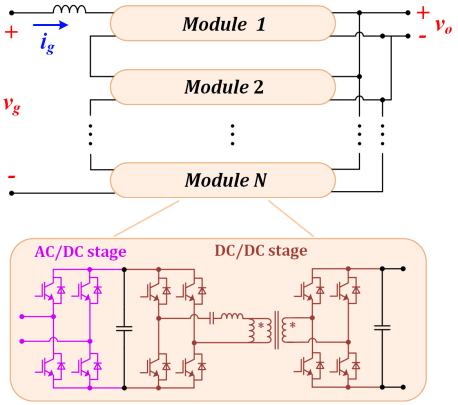

Fig. 1. Configuration 1: a typical configuration of PETT with CHB-based modular series-parallel structure.

In this case, using the low-voltage IGBTs to replace the high-voltage IGBTs seems like a solution. [20] points out that power semiconductors with blocking voltages of 1200 V or 1700 V have been identified to get optimum results in terms of efficiency and power density. However, using the low-voltage IGBTs means more power modules. Furthermore, the number of medium-frequency transformers (MFTs) will increase, whose high-voltage isolation design will restrict the improvement of the power density and increase costs. To further optimize the number and the characteristics of the MFTs, a multi-winding MFTs structure is proposed in [21], however, the power decoupling is relatively complex according to [8]. Additionally, a diode-clamped three-level multi-module PET system is developed in [22], which can help reduce MFT's number. Nevertheless, power level, unbalanced voltage, and switching losses are challenging for diode-clamped converters.

From above of view, the aim of this paper is thus to propose a PETT configuration, which can help use the low-voltage IGBTs (1700V or 1200V) to replace the high-voltage IGBTs (6500V or 3300V) and simplify the control system. Meanwhile, the number of the MFTs will not increase and ZCS or ZVS for all the IGBTs can be guaranteed. Then a comprehensive optimization of PETT, including switching losses, the number of MFTs and switches, and costs, can be finally achieved. The sections of this paper are organized as follows: Section II introduces the topology evolution from configuration 1 to the proposed PETT configuration 3. Section III analyzes the principle of the proposed PETT configuration and the corresponding control performance. In Section IV, the design method of the proposed PETT configuration is given and the performance comparisons are made. Section V verifies the validity of the proposed PETT configuration by an experimental prototype. Finally, Section VI concludes this paper.

II. Configuration And Topology Evolution Of PETT

To make a better understanding of PETT topology in the actual onboard traction system, the CRH380B EMUs of China is taken as an example to discuss how to replace conventional LFTT and 4QC with PETT. The rated input voltage is 25kV/50Hz. The rated power of each LFTT is about 5.8 MW, which is shared by two traction converters. So the power of each traction converter is about 2.9 MW. The rated output dc voltage of each traction converter is 3600 V. The structure of the traction unit is shown in Fig.2, where INV is the traction inverter and Motor represents the three-phase asynchronous motor. For each traction converter, the efficiency of LFTT is about 95% and of four-quadrant converters (4QC) is around 98%. Therefore, the total efficiency of LFTT and 4QC is about 93.1%.

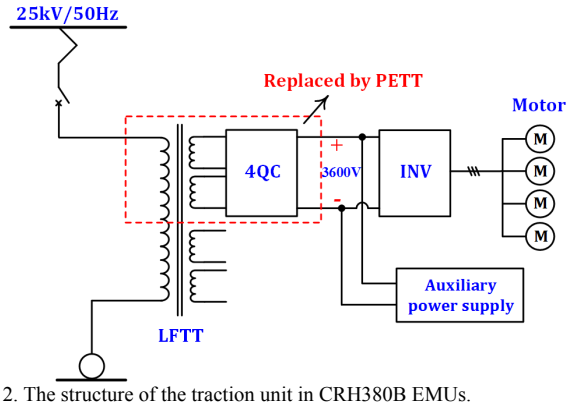

Fig. 2. The structure of the traction unit in CRH380B EMUs.

To replace a traction converter, including LFTT and 4QC, with a PETT, configuration 1 is preferred nowadays. For CRH380B EMUs, the total input voltage Vg is 25kV/50Hz, the desired DC output voltage is 3600V. If the number of the modules (N) in a PETT is selected as 12, the input power of each module is 243 kW, and the output voltages of AC/DC stage and DC/DC stage are all 3600 V. Thus 6.5 kV IGBT is selected. CHB converter is used as the AC/DC stage to provide a constant dc output. LLC resonant converter is usually used as the DC/DC stage to achieve the electrical isolation and high efficiency. Of course, low-voltage IGBT can also be used by increasing modules, but at the same time, the number of MFTs will increase.

In [20], the relationship of normalized switching energy and rated blocking voltage of Si IGBT can be expressed as

$$K_{off}(V_B) = A_{off}V_B^2 + B_{off}V_B + C_{off} \quad (1)$$

$$K_{on}(V_B) = A_{on}V_B^2 + B_{on}V_B + C_{on} \quad (2)$$

$$K_{rec}(V_B) = A_{rec}V_B^2 + B_{rec}V_B + C_{rec} \quad (3)$$

The relation curves are shown in Fig.3. The formulas are derived by fitting many datasheets of different Si IGBTs and it can help rapidly calculate the losses of Si IGBTs without datasheets. In this formulas, V_B is the rated blocking voltage of Si IGBT; K_{off}, K_{on}, and K_{rec} (mJ/A) are normalized the turn-off loss, the turn-on loss of the IGBTs and the normalized reverse recovery loss of the diodes respectively. A_i. B_i, C_i ($i = off, on, rec$) are empirical constants that can be found in [20]. From Fig. 3, it can be seen that higher blocking voltage means higher switching loss. Therefore, for the current 6.5kV IGBT, the switching frequency cannot be selected too high due to the huge normalized switching loss. It means that the power density of MFT cannot be further improved by increasing working frequency.

This article has been accepted for publication in a future issue of this journal, but has not been fully edited. Content may change prior to final publication. Citation information: DOI 10.1109/TPEL.2018.2889107, IEEE Transactions on Power Electronics

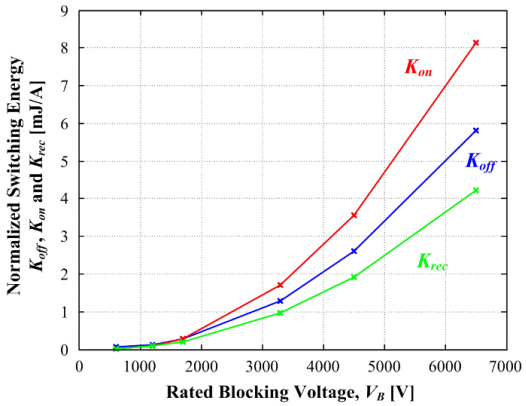

Fig. 3. The relationship of the normalized switching energy and the rated blocking voltage of Si IGBT.

To increase the switching frequency of the dc/dc stage in PETT, a configuration with input-series and output-series structure is proposed, which is shown in Fig. 4. For the sake of analysis, the configuration in Fig. 4 is called configuration 2. Compared with configuration 1, the single isolated dc/dc unit in each module is replaced with several input-series and output-series (ISOS) dc/dc units. If three dc/dc units are used in a dc/dc stage, the rated power of each unit is 81 kW and 1700 V Si IGBT can be used. If five dc/dc units are used in a dc/dc stage, the rated power of each unit is 48.6 kW and 1200 V Si IGBT can be used. When LLC resonant converter [23]-[26] is selected as the dc/dc unit, then the switching loss mainly comes from turn-off loss. Suppose that the turn-off current is i_{off}, then the turn-off energy loss E_{off} can be expressed as

$$E_{off} = K_{off} \cdot i_{off} \cdot \frac{u}{0.5} \tag{4}$$

Where u ($= V_{dc}/V_B$) represents the blocking voltage utilization, V_{dc} is the actual voltage stress of IGBT and V_B is the rated blocking voltage. Therefore, for the LLC resonant converter in Fig. 1, the turn-off loss of a 6.5 kV IGBT is calculated as $E_{off\_6.5kV} = i_{off} \cdot 6.3822$ (mJ). For the LLC resonant converter in Fig.4, if three units are used, the turn-off losses of three 1.7 kV IGBTs are calculated as $E_{off\_1.7kV} = i_{off} \cdot 1.05$ (mJ). If five units are used, the turn-off losses of five 1.2 kV IGBTs are calculated as $E_{off\_1.2kV} = i_{off} \cdot 0.7692$ (mJ). These results indicate that at the same switching frequency and turn-off current of LLC RC, the total turn-off losses of configuration 2 with three units and five units are 16.45% and 12.05% of configuration 1, i.e., the switching frequency can be improved at least 6 times theoretically by using configuration 2. However, the configuration 2 still has following limitations that will restrict its actual use.

1) There are too many high-frequency transformers in configuration 2. For onboard traction application, the isolated requirement of the transformers is very strict according to [6], [27]. For example, the test levels are 34.5 kVrms for the dielectric test and 75 kV for the basic impulse level test in 15 kV/16.7 Hz railway grid. The test levels are 60 kVrms (10 min) for the dielectric test and 150 kV for the basic impulse level test in 25 kV/50 Hz railway grid. Therefore, the size and costs of the isolating equipment will be large.
2) If the excitation currents of the MFTs are assumed constant, the copper losses of the MFTs will increase with the growing number of dc/dc units.
3) In configuration 2, ISOS dc/dc converters are used as a DC/DC stage, the power balance control should be considered. According to [28], the voltage balance control of ISOS structure is more difficult than input-series output-parallel (ISOP), input-parallel output-series (IPOS), and input-parallel output parallel (IPOP) structures, especially for bidirectional power conversion.

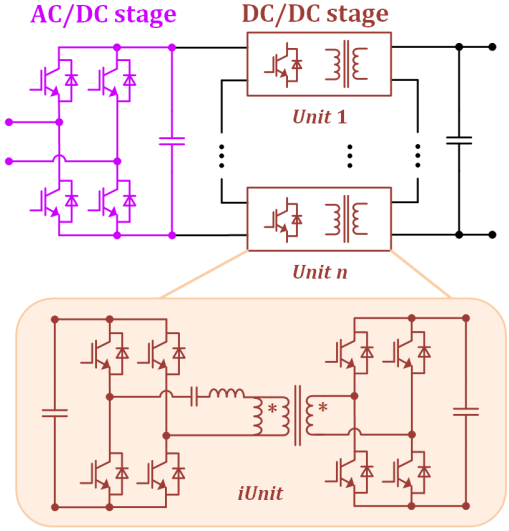

Fig. 4. Configuration 2: a dc/dc stage with ISOS structure.

To overcome the above three constraints, a voltage self-balancing resonant (VSBR) dc/dc converter is proposed to serve as the dc/dc stage, the corresponding PETT configuration is addressed as configuration 3. A three-capacitor VSBR dc/dc converter is shown in Fig. 5. Switching bridges (S_{p1a}, S_{p1b}), (S_{p2a}, S_{p2b}), (S_{p3a}, S_{p3b}) are in series with the input dc bus V_{in} and switching bridges (S_{q1a}, S_{q1b}), (S_{q2a}, S_{q2b}), (S_{q3a}, S_{q3b}) are in series with the output dc bus V_o. The resonant branches [(L_{p1}, C_{p1}), (L_{p2}, C_{p2})] are successively connected to the adjacent midpoints (P_1, P_2, and P_3) of (S_{p1a}, S_{p1b}), (S_{p2a}, S_{p2b}), and (S_{p3a}, S_{p3b}). The resonant branches [(L_{q1}, C_{q1}), (L_{q1}, C_{q1})] are successively connected to the adjacent midpoints (Q_1, Q_2, and Q_3) of (S_{q1a}, S_{q1b}), (S_{q2a}, S_{q2b}), (S_{q3a}, S_{q3b}). An LLC resonant converter is connected between the input capacitors C_{i2} and the output capacitors C_{o2}. Because of voltage self-balancing performance of the VSBR dc/dc converter, the input and the output voltage can be equally shared by the three input capacitors and three output capacitors. Thus, for this three-capacitor VSBR dc/dc converter, 1700 V IGBTs can be used. Of course, the number of the input and output capacitors can be adjusted freely. For example, five-capacitor VSBR dc/dc converter can also be used as the dc/dc stage and then 1200V IGBTs can be considered. The superiority of configuration 3 is that the high-voltage switches can be replaced with low-voltage switches to improve the switching frequency and increase efficiency. Meanwhile, the number of the MFTs can be reduced to one in each dc/dc stage, which will help simplify the isolation design of the transformers and save cost.

This article has been accepted for publication in a future issue of this journal, but has not been fully edited. Content may change prior to final publication. Citation information: DOI 10.1109/TPEL.2018.2889107, IEEE Transactions on Power Electronics

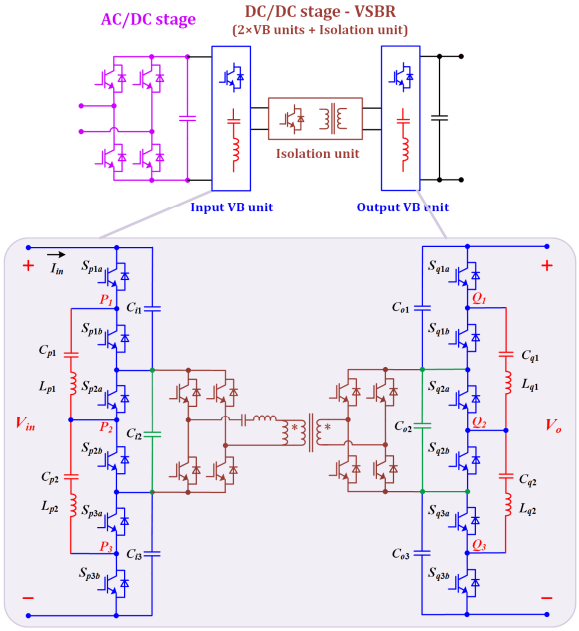

Fig. 5. Configuration 3: a dc/dc stage with a three-capacitor VSBR dc/dc converter.

III. Principle And Control Of VSBR DC/DC Converter

A. IVB and OVB Unit

From Fig. 5, VSBR dc/dc converter can be divided into three parts; input voltage balancing (IVB) unit, isolation unit, and output voltage balancing (OVB) unit.

The basic voltage-balance principle of IVB unit and OVB unit are similar to switched capacitor based power conversion, which are studied in [29]-[30]. In this paper, for the sake of analyzing the principle of IVB unit, other parts (including isolation unit and OVB unit) can be regarded as a load. Moreover, several assumptions should be provided as follows.

1) All the devices are ideal and the parasitic parameters can be ignored.

2) The resonant period of (L_{p1}, C_{p1}) and (L_{p2}, C_{p2})] is T_r, the switching period of (S_{p1a}, S_{p1b}), (S_{p2a}, S_{p2b}), and (S_{p3a}, S_{p3b}) is T_s, and the dead time of these switches is T_d.

3) The resonant time T_r is about equal to (T_s-2T_d).

The theoretical waveforms of a three-capacitor IVB unit are shown in Fig. 6. According to the theoretical waveforms, there are four working modes in a switching period.

Mode I (t_0-t_1): at t_0, S_{p1a}, S_{p2a}, and S_{p3a} are turned on, S_{p1b}, S_{p2b}, and S_{p3b} are off-state. Resonant capacitor C_{p1} is charged by DC capacitor C_{i1} through the loop that is consisted of S_{p1a}, L_{p1}, C_{p1}, and S_{p2a}. The resonant current i_{Lp1} will increase from 0 at t_0 and then oscillate back to 0 at t_1. At the same time, DC capacitor C_{i2} is charged by resonant capacitor C_{p2} through the loop, which is consisted of S_{p2a}, L_{p2}, C_{p2}, and S_{p3a}. The resonant current i_{Lp2} will reversely increase from 0 at t_0 and oscillate back to 0 at t_1. Thus, zero-current turn-on can be achieved for S_{p1a}, S_{p2a}, and S_{p3a} in this mode. The working principle schematic in Mode I is shown in Fig. 7(a) and the quantitative expressions are given as follows.

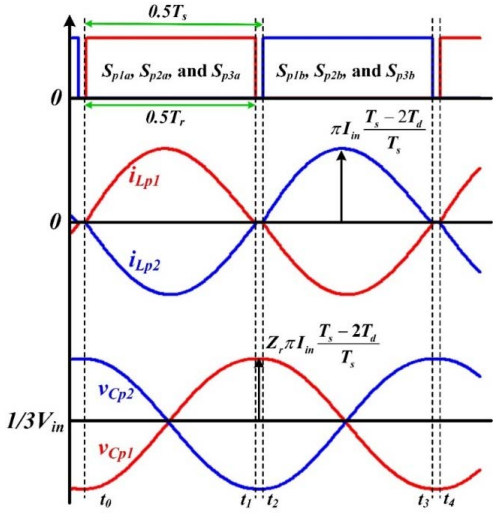

Fig. 6. The theoretical waveforms of a three-capacitor IVB unit.

$$
\begin{aligned}
i_{Lp1}(t) &= \pi I_{in}\frac{T_s-2T_d}{T_s}\sin\left[\omega_r(t-t_0)\right]\\
i_{Lp2}(t) &= -\pi I_{in}\frac{T_s-2T_d}{T_s}\sin\left[\omega_r(t-t_0)\right]\\
V_{Cp1}(t) &= V_{Ci2}-Z_{r1}\pi I_{in}\frac{T_s-2T_d}{T_s}\cos\left[\omega_r(t-t_0)\right]\\
V_{Cp2}(t) &= V_{Ci2}+Z_{r2}\pi I_{in}\frac{T_s-2T_d}{T_s}\cos\left[\omega_r(t-t_0)\right]
\end{aligned}
\tag{5}
$$

Where $Z_{r1}=\sqrt{L_{p1}/C_{p1}}$, $Z_{r2}=\sqrt{L_{p2}/C_{p2}}$. I_{in} is the input current of the IVB unit. The value of the peak current in (5) can be derived as follow. In a half period (0-0.5T_s), C_{i1} is discharged by the resonant branch and the discharging current is $i_{Lp1}(t)$. According to the charge conservation law, $I'_{in}\cdot T_s=\int_0^{0.5T_s} i_p(t)dt$. Suppose that the discharging current $i_{Lp1}(t)$ is a sinusoidal current, which can be represented by $i_p(t)=I_{Lp1}\cdot\sin(\omega_r t)$. Then the peak value I_{Lp1} can be calculated as $I_{Lp1}=\pi I_{in}\frac{T_s-2T_d}{T_s}$.

Mode II (t_1-t_2): at t_1, S_{p1a}, S_{p2a}, and S_{p3a} are turned off. Due to the resonant currents i_{Lp1} and i_{Lp2} have oscillated back to 0, zero-current turn-off can be achieved for S_{p1a}, S_{p2a}, and S_{p3a}. During this mode, all the switches are off state and only the output dc capacitor C_{i2} provides power to the load.

Mode III (t_2-t_3): at t_2, S_{p1b}, S_{p2b}, and S_{p3b} are turned on, S_{p1a}, S_{p2a}, and S_{p3a} are off state. DC capacitor C_{i2} is charged by resonant capacitor C_{p1} through the loop, which is consisted of S_{p1b}, L_{p1}, C_{p1}, and S_{p2b}. The resonant current i_{Lp2} will reversely increase from 0 at t_2 and oscillate back to 0 at t_3. Meanwhile, resonant capacitor C_{p2} is charged by DC capacitor C_{i3} through the loop that is consisted of S_{i2b}, L_{p3}, C_{p3}, and S_{p3b}. The resonant current i_{Lp2} will increase from 0 at t_2 and then oscillate back to 0 at t_3. Therefore, zero-current turn-on can be achieved for S_{p1b}, S_{p2b}, and S_{p3b} in this mode. The working principle schematic in Mode III is shown in Fig. 7(b) and the quantitative expressions are given as follows.

This article has been accepted for publication in a future issue of this journal, but has not been fully edited. Content may change prior to final publication. Citation information: DOI 10.1109/TPEL.2018.2889107, IEEE Transactions on Power Electronics

$$
\begin{aligned}
i_{Lp1}(t) &= -\pi I_{in}\frac{T_s-2T_d}{T_s}\sin\left[\omega_r(t-t_2)\right]\\
i_{Lp2}(t) &= \pi I_{in}\frac{T_s-2T_d}{T_s}\sin\left[\omega_r(t-t_2)\right]\\
V_{Cp1}(t) &= V_{Ci2}+Z_{r1}\pi I_{in}\frac{T_s-2T_d}{T_s}\cos\left[\omega_r(t-t_2)\right]\\
V_{Cp1}(t) &= V_{Ci2}-Z_{r2}\pi I_{in}\frac{T_s-2T_d}{T_s}\cos\left[\omega_r(t-t_2)\right]
\end{aligned}
\tag{6}
$$

Mode IV (t_3-t_4): at t_3, S_{p1b}, S_{p2b}, and S_{p3b} are turned off. Due to the resonant currents i_{Lp1} and i_{Lp2} have oscillated back to 0, zero-current turn-off can be achieved for S_{p1b}, S_{p2b}, and S_{p3b}. Like Mode II, all the switches are off state and only the output dc capacitor C_{i2} provides power to the load during this mode. In the same way, the principle of OVB unit can be analyzed by regarding IVB unit and isolation unit as an input dc source. The main working principle schematics are shown in Fig. 8. Since the working modes are similar to the IVB unit, the analysis of the working modes is not shown here. According to Fig. 6, it can be seen that the duty ratio and frequency of the drive pulses for IVB and OVB unit are fixed. If the dead time is ignored, the complementary drive pulses with 50% duty ratio are used for each half-bridge, and the drive pulses of all the half-bridges are synchronous, which is shown in TABLE I.

TABLE I
THE DRIVE PULSES OF ALL THE HALF BRIDGES

Time	S_{p1a}, S_{p2a}, and S_{p3a} S_{q1a}, S_{q2a}, and S_{q3a}	S_{p1b}, S_{p2b}, and S_{p3b} S_{q1b}, S_{q2b}, and S_{q3b}
$0\sim(0.5T_s\text{-}T_d)$	on	off
$(0.5T_s\text{-}T_d)\sim 0.5T_s$	off	off
$0.5T_s\sim(T_s\text{-}T_d)$	off	on
$(T_s\text{-}T_d)\sim T_s$	off	off

According to the above analysis, for IVB unit, the power in C_{i1} and C_{i3} is transferred to C_{i2} in a switching period. For OVB unit, the power in dc capacitors in C_{o2} is transferred to C_{o1} and C_{o3} in a switching period. Thus, a power sharing can be achieved for these dc capacitors. Taking the IVB unit in Mode I as an example, suppose that the voltage of C_{i1} is a constant dc value and without any ripple. According to the fundamental resonant principle, when the resonance is in steady state, the voltage of resonant capacitor C_{p1} can be expressed as

$$
v_{Cp1}(t) = V_{Ci1}+\left(v_{Cp1}(t_0)-V_{Ci1}\right)\cdot\cos\left[\omega_r(t-t_0)\right]+Z_r i_{Lp1}(t_0)\cdot\sin\left[\omega_r(t-t_0)\right] \tag{7}
$$

Where V_{Ci1} is the voltage of C_{i1}, $v_{Cp1}(t_0)$ and $i_{Lp1}(t_0)$ are the initial voltage of C_{p1} and the initial current of L_{p1} at t_0, respectively. According to (5), $V_{Cp1}(t_0)=V_{Ci2}-Z_r\pi I_{in}\frac{T_s-2T_d}{T_s}$ and $i_{Lp1}(t_0)=0$. Then the voltage of resonant capacitor C_{p1} can be finally shown as

$$
v_{Cp1}(t) = V_{Ci1}+\left(V_{Ci2}-Z_r\pi I_{in}\frac{T_s-2T_d}{T_s}-V_{Ci1}\right)\cdot\cos\left[\omega_r(t-t_0)\right] \tag{8}
$$

Combine (5) with (8), it can be acquired that $V_{Ci1} = V_{Ci2}$. Similarly, $V_{Ci3} = V_{Ci2}$ can be derived in Mode III and then $V_{Ci1} = V_{Ci2} = V_{Ci3}$ is proved. In the same way, $V_{Co1} = V_{Co2} = V_{Co3}$ can be derived. Therefore, for IVB and OVB unit, the voltage balance of the dc capacitors can be automatically guaranteed.

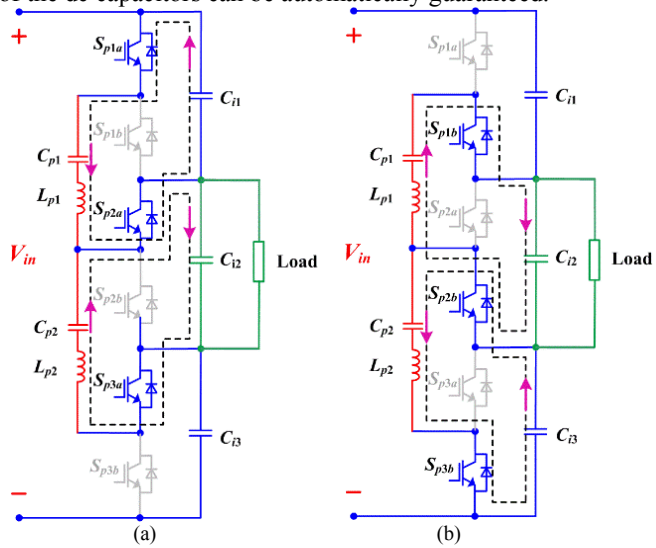

Fig. 7. The working principle schematic of IVB unit: (a) Mode I, (b) Mode III.

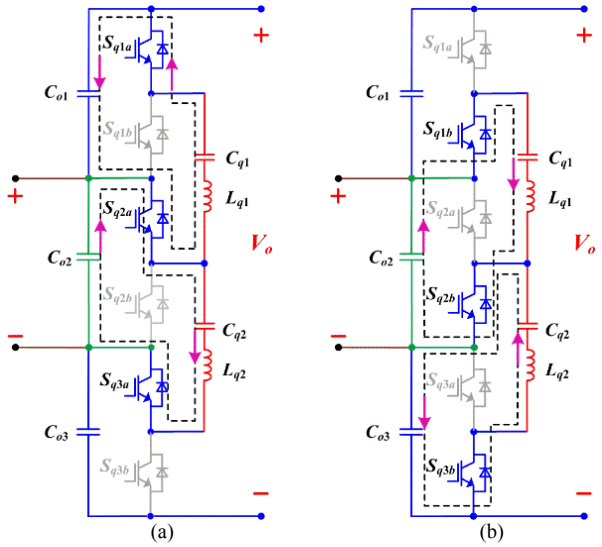

Fig. 8. The working principle schematic of OVB unit: (a) Mode I, (b) Mode III.

B. Isolation Unit

For isolation unit, any bidirectional isolated dc/dc converter can be used. Usually, soft-switching dc/dc converters are highly recommended, such as LLC resonant converter and dual-active-bridge (DAB) converter. These two converters have different characteristics. Generally speaking, LLC converter has lower switching losses and DAB converter has better power management ability. For the PETT application, LLC resonant converter is usually more preferred because that high efficiency and high switching frequency are the primary factors to be considered in the design procedure [18]. Therefore, LLC resonant converter is selected as the isolation unit in this paper.

C. Control Strategy

For the sake of analyzing the control, the schematics of the three given configurations are all shown in Fig.9. It can be seen that the numbers of the PETT modules are equal at the same

This article has been accepted for publication in a future issue of this journal, but has not been fully edited. Content may change prior to final publication. Citation information: DOI 10.1109/TPEL.2018.2889107, IEEE Transactions on Power Electronics

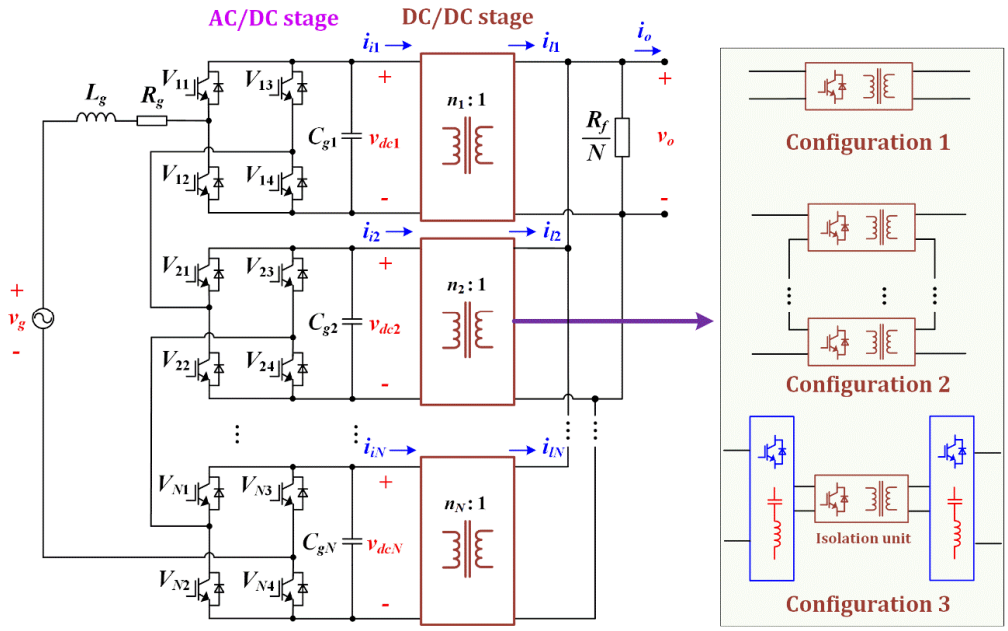

Fig. 9. The schematics of the three given configurations.

working situation, and CHB structure is used for the AC/DC stage. The difference of the three configurations is mainly from DC/DC stage. For configuration 1, a single DC/DC converter is used in each module. For configuration 2, an ISOS DC/DC converter is used in each module. For configuration 3, a VSBR dc/dc converter is used in each module.

If the difference of the three PETT configurations in DC/DC stage is not considered, they all can be regarded as the traditional modular AC/DC SST. To get desired voltage, current and achieve the power balance of the different modules, many control strategies have been studied and presented by many experts and scholars [19],[31]-[32]. However, for configuration 2 and 3, except for the overall control of the modules, the power balance control in each DC/DC module should also be considered. For configuration 2, because ISOS structure is used in the DC/DC module, the power balance must be achieved, i.e. input voltage sharing (IVS) control [33] or current-mode IVS control [34] should be used. Thus, a double power balance control will be used for configuration 2 (overall control for all the modules and inside power balance control for each DC/DC module), which will complicate the control strategy. For configuration 3, extra power balance control is not necessary since the IVB unit and OVB unit can directly guarantee the voltage balance of the input and output voltage of each DC/DC. Thus, compared with configuration 2, the control strategy of configuration 3 is simpler because of the voltage self-balancing capability of each DC/DC module.

Besides, it is very simple for the VSBR converter to start up. Before the input voltage is applied, the complementary drive pulses with 50% duty ratio should be applied for each half-bridge. With the increasing of the input voltage, the soft start of the VSBR can be achieved. Fig. 10 shows the simulation results of the start-up process for a three-capacitor VSBR dc/dc converter (shown in Fig. 5). The simulation parameters are listed in TABLE II. First, the input voltage increases to 3600V gradually. After 0.1s, the input voltage keeps constant. During the whole start-up process, the input voltage of IVB unit and OVB unit can always keep balance, and their resonant currents increase slowly. Therefore, a soft start of the VSBR can be achieved easily.

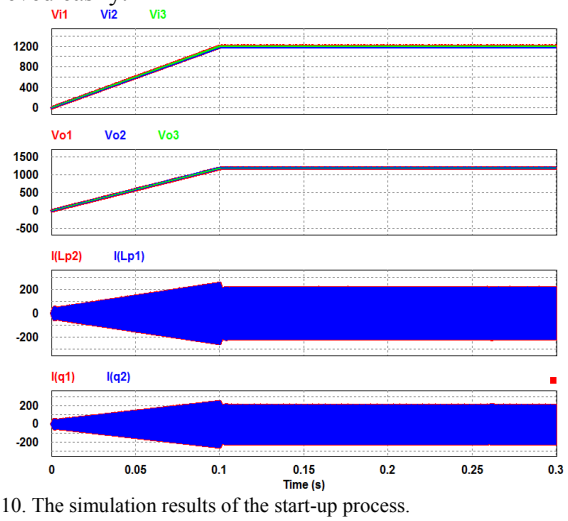

Fig. 10. The simulation results of the start-up process.

TABLE II
THE SIMULATION PARAMETERS

Parameters	Values
Input dc voltage V_{in}	3600V
Output dc voltage V_o	3600V
Rated power	243 kW
Switching frequency	20 kHz

IV. PERFORMANCE AND DESIGN OF THE VSBR DC/DC CONVERTER

A. Voltage Balance Performance

This article has been accepted for publication in a future issue of this journal, but has not been fully edited. Content may change prior to final publication. Citation information: DOI 10.1109/TPEL.2018.2889107, IEEE Transactions on Power Electronics

In the above analysis, the parasitic parameters of IVB and OVB unit are neglected and all the switches are regarded as ideal. However, in reality, the equivalent series resistance (ESR) will produce voltage drop so the voltage difference of C_{i1}, C_{i2}, C_{i3} or C_{o1}, C_{o2}, C_{o3} will occur. Considering the IVB unit, suppose that R_{p1} and R_{p2} are the ESR of the two resonant branches. R_s is the ESR of each switch. According to (7), the root mean square (RMS) value of the resonant current can be derived as

$$I_{Lp1-rms} = I_{Lp2-rms} = \frac{\pi}{\sqrt{2}}\sqrt{\frac{T_s}{T_s - 2T_d}}I_{in} \tag{9}$$

Then the total losses of resonant branches and switches can be calculated as

$$P_{loss} = I_{Lp1-rms}^2\left(R_{p1}+2R_s\right) + I_{Lp2-rms}^2\left(R_{p2}+2R_s\right) = \frac{\pi^2}{2}\frac{T_s}{T_s-2T_d}I_{in}^2\left(R_{p1}+R_{p2}+4R_{esr\_s}\right) \tag{10}$$

To calculate the voltage difference, an equivalent loss schematic is shown in Fig. 11. R_{esr} is used to represent the loss caused by parasitic parameters. According to (10), R_{esr} can be finally expressed as

$$R_{esr} = \frac{\pi^2}{2}\frac{T_s}{T_s-2T_d}\left(R_{p1}+R_{p2}+4R_s\right) \tag{11}$$

Then the voltage of C_{i2} is $\frac{1}{3}\left(V_{in} - I_{in}R_{esr}\right)$, the voltage of C_{i1} and C_{i3} is $(\frac{1}{3}V_{in} + \frac{1}{6}I_{in}R_{esr})$. The difference between C_{i1} (or C_{i3}) and C_{i2} is shown as

$$\Delta V = V_{C_{i1}} - V_{C_{i2}} = 0.5\, I_{in}R_{esr} \tag{12}$$

If the switches are decided, R_s is usually constant. Thus, to reduce the voltage difference, the most effective way is to reduce the ESR of the resonant branches. Of course, in practical applications, R_{esr} is usually very small so the voltage difference is not very large, which usually can meet the requirements for most applications. For example, when the parameters are chosen as TABLE II, and the R_{esr} is set as 100mΩ. Then the difference between the DC capacitors is 3.375V, which is an acceptable value in such power level.

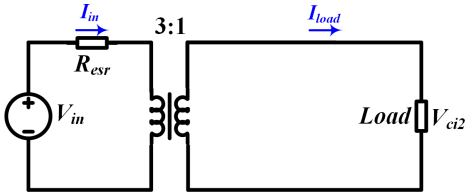

Fig. 11. The equivalent loss schematic.

B. Design of the Resonant Branches

When design the resonant branches of the IVB and OVB, many aspects should be considered. First, the resonant frequency of the resonant branches should be decided, which is about equal to the switching frequency f_s. According to the resonant principle, we can get $\sqrt{L_pC_p} = \frac{1}{2\pi f_s}$. Then the voltage and current stress of the resonant branch should be analyzed. From (5) and (6), the peak value of the resonant current I_{pm}, inductor voltage V_{Lpm}, and capacitor voltage V_{Cpm}, which shown in Fig. 6, can be derived as

$$I_{pm} = \pi I_{in}\frac{T_s - 2T_d}{T_s} \tag{13}$$

$$V_{Lpm} = \frac{1}{\sqrt{L_pC_p}}\pi I_{in}\frac{T_s-2T_d}{T_s} = 2\pi^2 I_{in}\frac{T_s-2T_d}{T_s^2} \tag{14}$$

$$V_{Cpm} = \frac{1}{3}V_{in} + Z_p\pi I_{in}\frac{T_s-2T_d}{T_s} \tag{15}$$

From (13) and (14), it can be seen that the current and voltage stress of the inductor is constant if the input power is decided. Different inductance and capacitance mainly influence the voltage stress of the resonant capacitor according to (15). As for the IVB, if $V_{Cpm} > V_{Ci1} + V_{Ci2} = \frac{2}{3}V_{in}$ or $V_{Cpm} > V_{Ci2} + V_{Ci3} = \frac{2}{3}V_{in}$, extra resonant circuits will occur, which is shown in Fig. 12. The extra resonant circuits will disturb the normal operation and ZCS may not be achieved. Thus, to avoid redundant working modes, the peak value of the capacitor voltage must meet $V_{Cpm} < \frac{2}{3}V_{in}$. Substitute (15) into $V_{Cpm} < \frac{2}{3}V_{in}$, the following inequality can be obtained as

$$Z_p < \frac{V_{in}}{3\pi I_{in}}\cdot\frac{T_s}{T_s-2T_d} \tag{16}$$

Connect (16) and $\sqrt{L_pC_p} = \frac{1}{2\pi f_s}$, the upper limit of the inductance can be expressed as $L_p < \frac{V_{in}}{6\pi^2 I_{in}}\cdot\frac{T_s^2}{T_s-2T_d}$.

According to the above analysis, it seems that smaller L_p can keep IVB or OVB away from redundant working modes and get a smaller voltage ripple of C_p. However, due to the parasitic resistance of the resonant capacitor and inductor, L_p can not be very small. Suppose the parasitic resistance is R_p, then the actual resonant frequency can be expressed as

$$f_p = \frac{1}{2\pi\sqrt{\frac{1}{L_pC_p} - \left(\frac{R_p}{2L_p}\right)^2}} \tag{17}$$

To guarantee that the resonant frequency is not influenced by the parasitic resistance, the following inequality should be guaranteed

$$\frac{1}{L_pC_p} >> \left(\frac{R_p}{2L_p}\right)^2 \tag{18}$$

Let $\frac{1}{L_pC_p} > 100\cdot\left(\frac{R_p}{2L_p}\right)^2$, then the lower limit of the inductance can be expressed as $L_p \geq \frac{2.5R_p}{\pi f_p}$. According to the analysis, the value range of the resonant inductor is

$$\frac{2.5R_p}{\pi f_s} \leq L_p < \frac{V_{in}}{6\pi^2 I_{in}}\cdot\frac{T_s^2}{T_s-2T_d} \tag{19}$$

Similarly, take the parameters in TABLE. II as an example, the range of the resonant inductor is $3.9\mu H \leq L_p \leq 48.9\mu H$. Then the range of resonant capacitor can be expressed as $1.3\mu F \leq L_p \leq 16.24\mu F$. By observing the value range of the

This article has been accepted for publication in a future issue of this journal, but has not been fully edited. Content may change prior to final publication. Citation information: DOI 10.1109/TPEL.2018.2889107, IEEE Transactions on Power Electronics

resonant branches, they do not need complicated isolation design and they are all small and easy to select compared with the isolated transformers. In general, the resonant capacitor should be priority selected, because capacitors are industrialized and the value is specific. Then the resonant inductor can be determined based on the value of resonant capacitor. The selection of the resonant branches is comprehensive. Small L_p can help avoid extra working modes and reduce the voltage ripple of the capacitor. Large L_p can help avoid the influence of parasitic resistance and reduce the inrush current during start up stage.

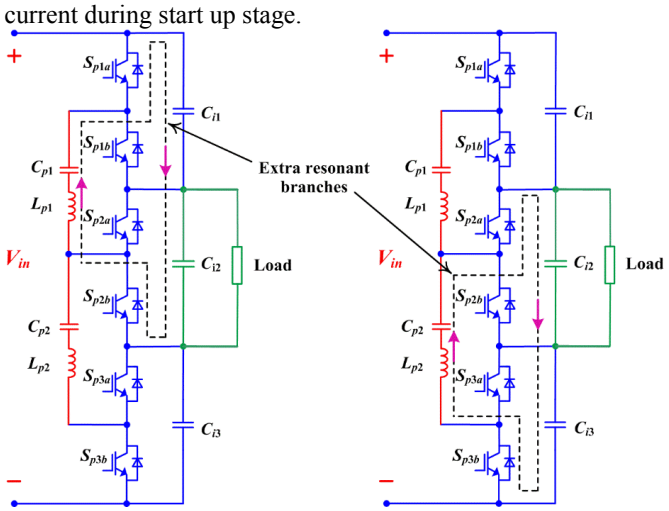

Fig. 12. The extra resonant circuits.

C. Performance Comparison

In this paper, three kinds of PETT configurations are presented. They are all two-stage structures, which consist of an AC/DC stage and a DC/DC stage. In AC/DC stage, the topologies of the three configurations are in common and CHB converter is used, while the topologies are different in the DC/DC stage. Single dc/dc converter is used in configuration 1, which is shown in Fig. 1. ISOS DC/DC converter is used in configuration 2, which is shown in Fig. 4. VSBR DC/DC converter is used in configuration 3, which is shown in Fig. 5. In addition, considering that NPC or flying-capacitor bridge legs as a DC/DC converter in the cascaded cells is a well-known approach to reduce voltage stress and the number of cascaded cells transformers, a comparison with a multilevel LLC resonant is made. To analyze the losses of these topologies, the CRH380B EMUs are still taken as an example, whose input power of each module is 243 kW, the output voltages of AC/DC stage and DC/DC stage are 3600 V. According to the applications, the three configurations are organized as follow. In configuration 1, only a single LLC RC is used in a DC/DC module. In configuration 2, ISOS DC/DC converter with three units is used in each DC/DC module. In configuration 3, the three-capacitor VSBR DC/DC converter is used in a DC/DC module. Finally, a five-level LLC flying-capacitor topology, which is proposed in [35], is used in a DC/DC module as a comparison. For the sake of calculation, the following assumptions are made. 1) LLC RC is selected as the basic topology in these configurations. 2) The transformers' parameters of the three configurations are in common and the efficiency of the high-frequency transformer is set as 99.4% according to [25], and the difference of the copper losses for these topologies is ignored. 3) The switching frequency of the three configurations is 20 kHz. 4) The rated power of each DC/DC module is 243kW. Then the calculated losses of the three configurations are all shown in TABLE III.

It should be pointed that the influence of the stored charge in the devices is not considered, and the relevant contents can be referred to [36]. From TABLE. III, if the 6.5kV Si IGBT is applied to DC/DC stage at 20 kHz, the total loss can reach to 16.134 kW, which will influence the normal working of the IGBT. That is why configuration 1 cannot work at high switching frequency. Compared with configuration 1, the total losses of configuration 2 and 3 can be highly reduced. That is to say, the total loss can be efficiently reduced by using low voltage device to replace high voltage device. In configuration 2, the total loss is mainly from switching loss because of many ISOS units. In configuration 3, the total loss mainly comes from conduction loss because of using IVB units and OVB units. In general, the switches with lower turn-off losses should be selected for configuration 2. While for configuration 3, the switches with lower conduction losses may be preferred. As for the five-level LLC flying-capacitor topology, the current stress is higher than other configurations, which causes higher conduction losses. For further discussing the performance of the DC/DC stage of the three configurations, some comparative results are given in TABLE IV, which contains the voltage / current (V/C) stresses of IGBTs, the number and type of IGBTs, the number of DC capacitors, the estimated costs of IGBTs and the drivers, the number of transformers, and whether needs IVS control for each DC/DC module.

In TABLE. IV, the costs of the corresponding IGBTs and their drivers can be searched in [37]. It should be pointed out that the costs are estimated and have difference in different country. Therefore, the estimated costs are for reference only. Even though the number of IGBTs in configuration 2, configuration 3, and five-level LLC topology are more than configuration 1, the total costs of the IGBTs are lower, especially for configuration 2 and 3. In the aspects of IGBT's number and costs, the performance of configuration 2 and 3 is similar. However, there are too many transformers in configuration 2. It will complicate the isolation design, increase transformer losses. In addition, more transformers mean more costs. For example, the quotation of a medium frequency transformer is about $4700, whose rate power is 200 kVA and the dielectric test is 20 kV rms. The price will increase further in onboard traction application because of higher isolation requirement. As for configuration 3 and five-level LLC flying-capacitor topology, only one transformer is needed and thus they may be more preferred in onboard traction application. However, compared with configuration 3, the five-level LLC flying-capacitor topology has the following drawbacks: 1) The current stress is very high, which will lead large losses; 2) more bulky DC capacitors are used, which will increase the power density and costs; 3) the control logic is complex. Moreover, the on-off time of the IGBTs is different, which may lead to thermal unbalance; 4) the control performance of the voltage balance and bidirectional power flow is poorer than the three configurations. Thus, configuration 3 will be a good choice for PETT. For the sake of a comprehensive comparison of these

This article has been accepted for publication in a future issue of this journal, but has not been fully edited. Content may change prior to final publication. Citation information: DOI 10.1109/TPEL.2018.2889107, IEEE Transactions on Power Electronics

TABLE III
THE LOSSES OF THE THREE CONFIGURATIONS

			Conduction loss (kW)	Switching loss (kW)	Transformer loss (kW)	Total loss (kW)	Efficiency (%)
Each AC/DC stage			0.231	2.868		3.099	98.69
Each DC/DC stage	Configuration 1	6.5 kV Si IGBT	0.304	14.39	1.44	16.134	93.20
	Configuration 2	1.7 kV Si IGBT	0.468	1.878	1.44	3.786	98.42
	Configuration 3	1.7 kV Si IGBT	1.368	0.626	1.44	3.434	98.57
	Five-level LLC	1.7 kV Si IGBT	2.29	1.17	1.44	4.9	97.96

TABLE. IV
THE COMPARATIVE DIAGRAM OF THREE PROPOSED CONFIGURATIONS

DC/DC stage	V/C stresses of IGBTs		IGBT	No. of DC capacitors (1.4kV)	Estimated costs of IGBTs and the drivers	No. of transformers	IVS for each module
Configuration 1	V_N/I_N		8×N FZ250R65KE3	6×N	$(8999.44+1880)×N	1×N	No
Configuration 2	$\frac{1}{3}V_N/I_N$		24×N FF150R17KE4	6×N	$(1219.2+1380)×N	3×N	Yes
Configuration 3	IVB&OVB	LLC	20×N FF450R17KE3	6×N	$(2725.3+1050)×N	1×N	No
	$\frac{1}{3}V_N/\frac{\pi}{\sqrt{2}}I_N$	$\frac{1}{3}V_N/3I_N$					
Five-level LLC	Primary side	Secondary side	16×N FF800R17KE3	12×N	$(7280.8+920) ×N	1×N	Yes
	$\frac{1}{4}V_N/8I_N$	$\frac{1}{4}V_N/4I_N$					

*N represents the number of the PETT module. The driver 1SC0450 is used for 6.5kV IGBT, 2SC0435T is used for 1.7kV IGBT.

configurations, a visual diagram is given in Fig. 13, which contains losses, numbers of transformers and IGBTs, and costs. By normalization processing, all the data of configuration 1 is regarded as one and smaller area means better merit. From Fig. 13, configuration 3 encircles the smallest area. Therefore, configuration 3 will be a better choice in onboard traction application.

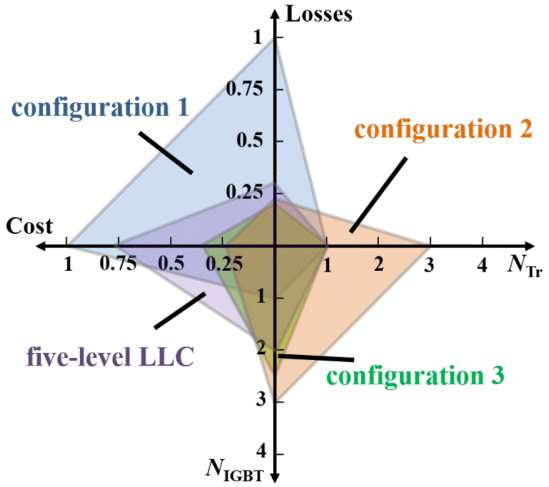

Fig. 13. The performance diagram of the three PETT configurations.

V. EXPERIMENTAL RESULTS

To verify the correctness of the above analysis about configuration 3, a 6 kW experimental platform is built. The corresponding circuit schematic is shown in Fig. 14, which is one module of PETT and consists of a single-phase rectifier and a VSBR DC/DC converter. The VSBR DC/DC converter is composed of a three-capacitor IVB, a full-bridge LLC resonant converter, and a three-capacitor OVB. The direction of the arrow in Fig. 14 is defined as the positive direction of the current. The experimental parameters are listed in TABLE IV. The picture of the platform is shown in Fig. 15, in which the control circuit is composed of a master controller and several slave controller. The master controller (including a DSP and an FPGA) is used to sample, calculation, communication, and protection. The slave controllers are used for generating PWM pulses and protection.

Fig. 16 indicates the dynamic waveforms of configuration 3, in which the output power is changed from 2.5 kW to 5 kW and then from 5 kW to 6 kW. In Fig. 16(a), the voltages of the three medium dc capacitors (V_{Ci1}, V_{Ci2}, and V_{Ci3}) and one of the resonant current of the resonant branch (L_{p1} and C_{p1}) are given. According to the results, the voltage balance of C_{i1}, C_{i2}, and C_{i3} can be always achieved at different power points. In Fig. 16 (b), the dynamic waveform of the LLC resonant control is presented. V_{Ci2} and V_{Co2} are the input voltage and the output voltage, respectively. I_r is the primary resonant current. From the experimental results, the LLC resonant converter works at the fixed-frequency (near the resonant frequency) and thus the gain can be regarded as a constant value. The three output dc capacitors (V_{Co1}, V_{Co2}, and V_{Co3}) and one of the resonant current of the resonant branch (L_{q1} and C_{q1}) is shown in Fig. 16(c). Similarly, When the VSBR converter works at different output power, the voltage balance of the three output dc capacitors can be guaranteed.

This article has been accepted for publication in a future issue of this journal, but has not been fully edited. Content may change prior to final publication. Citation information: DOI 10.1109/TPEL.2018.2889107, IEEE Transactions on Power Electronics

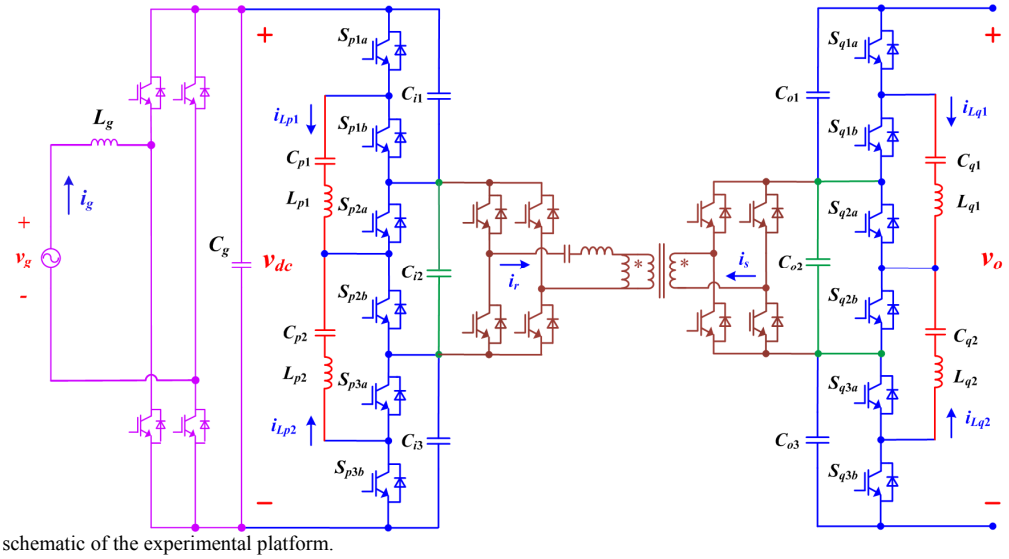

Fig. 14. The circuit schematic of the experimental platform.

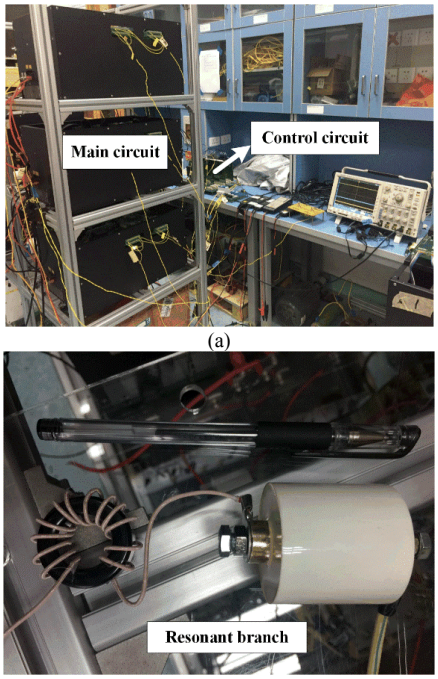

(a)

(b)

Fig. 15. The picture of the experimental platform.

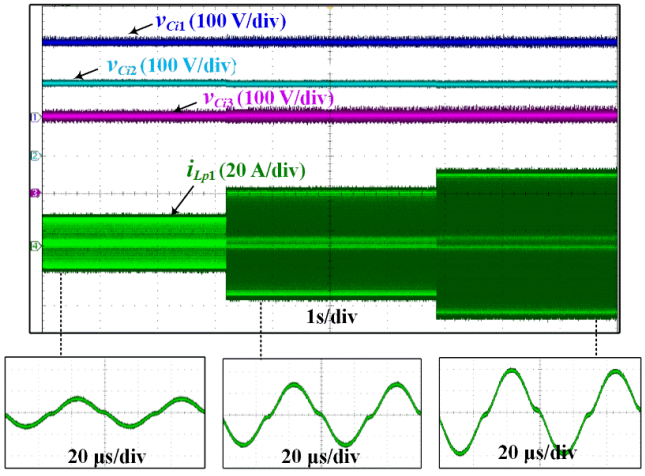

(a)

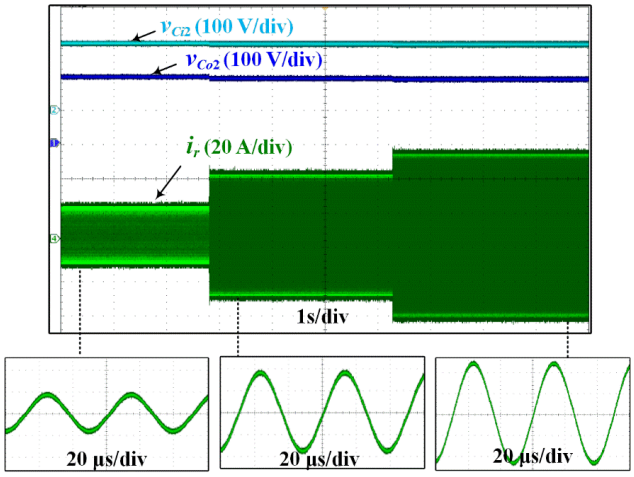

(b)

TABLE IV
THE EXPERIMENTAL PARAMETERS

Parameters	Values
Input ac voltage V_g	380V
Medium dc voltage V_{dc}	600 V
Output dc voltage V_o	600V
Resonant capacitors C_{p1} C_{p2} C_{q1} C_{q2}	10 μF
Resonant inductors L_{p1} L_{p2} L_{q1} L_{q2}	5 μH
Resonant capacitors C_r	2 μF
Resonant inductors L_r	31.5 μH
Rated power	6 kW
Switching frequency of DC/DC stage	20 kHz
Switching frequency of AC/DC stage	1250 Hz

This article has been accepted for publication in a future issue of this journal, but has not been fully edited. Content may change prior to final publication. Citation information: DOI 10.1109/TPEL.2018.2889107, IEEE Transactions on Power Electronics

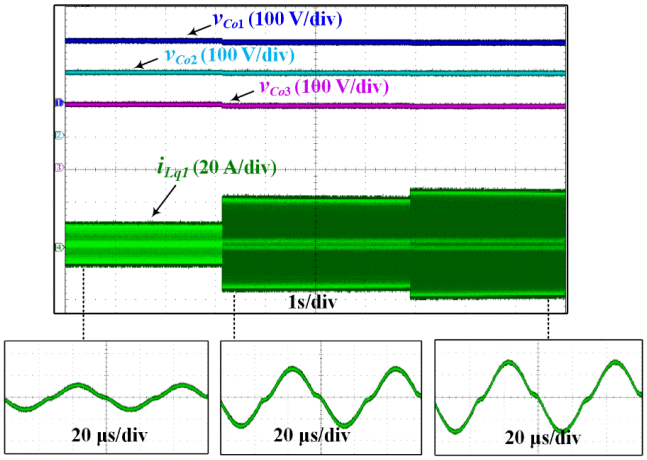

(c)

Fig. 16. The dynamic waveforms of configuration 3: (a) IVB unit; (b) LLC resonant converter; (c) OVB unit.

Fig. 17 shows the ZCS situation of the IVB unit. I_{Lp1} and I_{Lp2} are respectively the currents of L_{p1} and L_{p2}. V_{Sp1a} and V_{Sp3a} are respectively the voltage of S_{p1a} and S_{p3a}. It can be found that at different power points, the turn-on and turn-off currents are all about zero during the switching time. Thus, ZCS of S_{p1a}, S_{p2a}, and S_{p3a} can be achieved under any load condition. Moreover, the resonant current I_{Lp1} and I_{Lp2} flow through S_{p1a}, S_{p2a}, and S_{p3a} in a half switching period, and flow through S_{p1b}, S_{p2b}, and S_{p3b} in another half-switching period. According to the principle of symmetry, ZCS of S_{p1b}, S_{p2b}, and S_{p3b} can also be achieved.

The ZCS situation of the OVB unit is given in Fig. 18. I_{Lq1} and I_{Lq2} are respectively the currents of L_{q1} and L_{q2}. V_{Sq1a} and V_{Sq3a} are respectively the voltage of S_{q1a} and S_{q3a}. It also can be found that the turn-on and turn-off current is about zero during the switching time. Thus, ZCS of S_{q1a}, S_{q2a}, and S_{q3a} can be achieved under any load condition. Similarly, according to the principle of symmetry, ZCS of S_{q1b}, S_{q2b}, and S_{q3b} can be achieved, too.

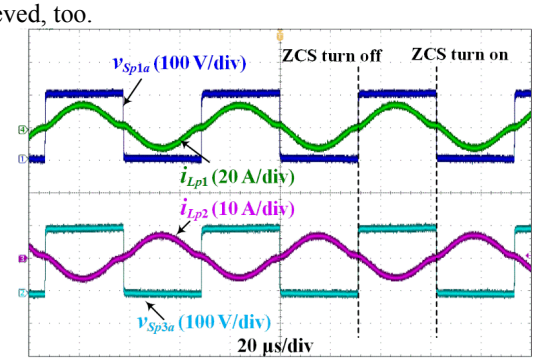

(a)

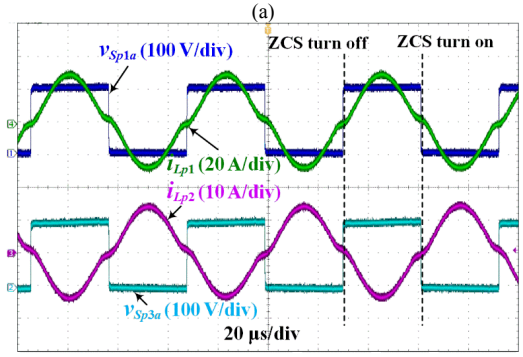

(b)

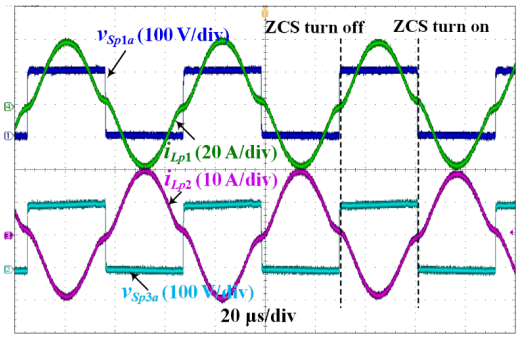

(c)

Fig. 17. The ZCS conditions of IVB unit: (a) 2 kW; (b) 5 kW; (c) 6 kW.

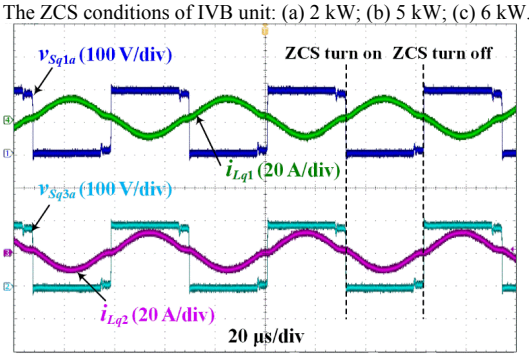

(a)

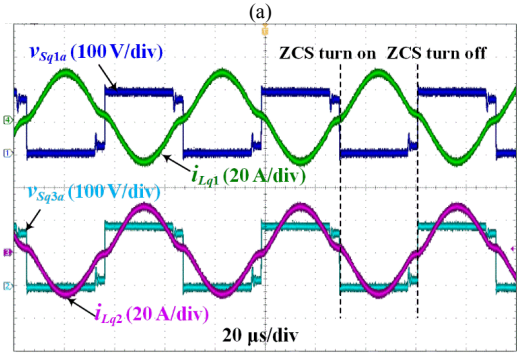

(b)

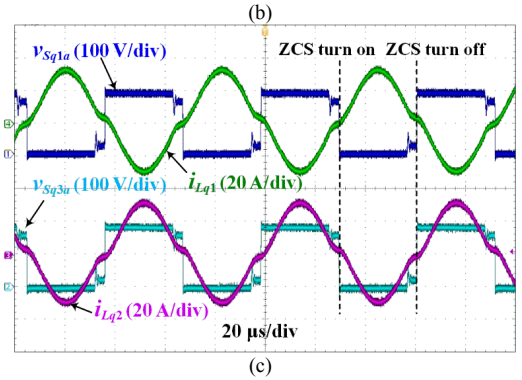

(c)

Fig. 18. The ZCS conditions of OVB unit: (a) 2 kW; (b) 5 kW; (c) 6 kW.

The experimental results of the single-phase rectifier are given in Fig. 19. By controlling the single-phase rectifier with the conventional voltage and current double closed-loop control method, the desirable output can be obtained at different load conditions.

This article has been accepted for publication in a future issue of this journal, but has not been fully edited. Content may change prior to final publication. Citation information: DOI 10.1109/TPEL.2018.2889107, IEEE Transactions on Power Electronics

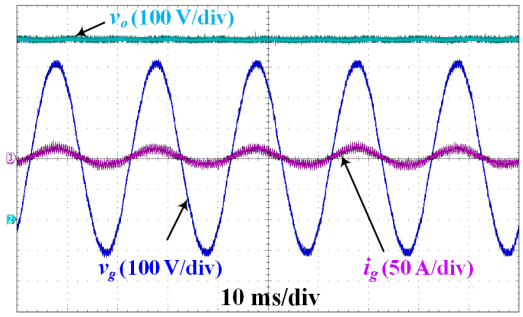

(a)

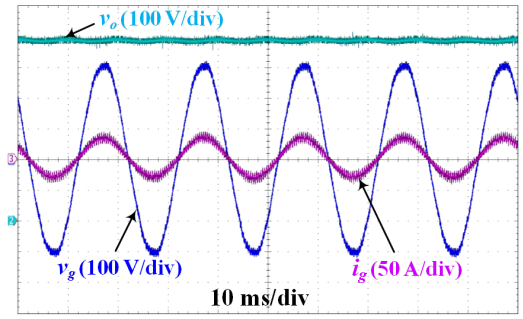

(b)

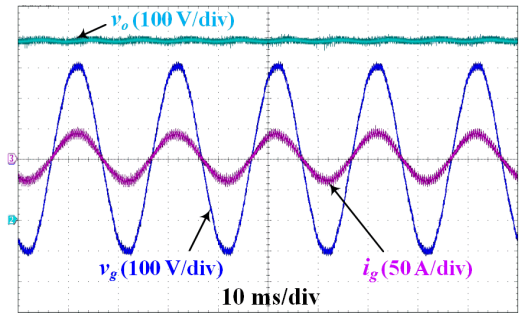

(c)

Fig. 19. The experimental results of the single-phase rectifier: (a) 2 kW; (b) 5 kW; (c) 6 kW.

Finally, the efficiency curves of configuration 2 and 3 are given in Fig. 20, which is the overall efficiency of a module (including AC/DC stage and DC/DC stage). From Fig. 20, it can be found that the efficiency of the two configurations at the rated power is similar. However, the efficiency of configurations 3 is higher than configuration 2 in light-load condition. That is because the turn-off current for LLC converters can be regarded as constant under all load conditions. Thus, the turn-off losses for LLC converters are high in light-load condition. Compared with configuration 3, configuration 2 has more LLC converters in a module, which will lead to lower efficiency in light-load condition. However, it should be pointed out that the efficiency in light-load condition can still be improved by using burst mode or reducing number of operating cells in light-load condition, which is discussed in [19].

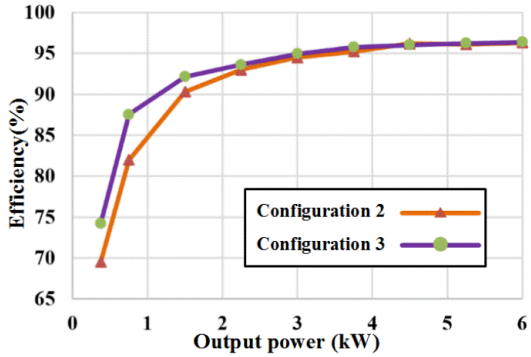

Fig. 20. The efficiency curves of configuration 2 and configuration 3.

VI. Conclusion

At present, the switching frequency, power density, efficiency, and costs are the main restrictions to use PET for the onboard traction applications. This paper proposes a PETT configuration for traction application with low-voltage IGBTs in the DC/DC stage. The characteristics of this configuration are as follows:

1) The high-voltage IGBTs can be replaced by low-voltage IGBTs, which can help increase switching frequency and reduce costs.
2) The numbers of the high-frequency transformers will not increase, which can further reduce costs, improve power density, and simplify isolation design.
3) ZCS or ZVS can be guaranteed for all the switches in the dc/dc stage, which can ensure high efficiency of the PETT.
4) The control strategy of the dc/dc module is simple because of the voltage self-balancing capability of the proposed VSBR converter.

These characteristics may eliminate the restrictions of the PETT, such as switching frequency, weight, volume, and costs, which makes the proposed PETT configuration superior and potential for the onboard traction applications. Moreover, the proposed configuration is not only suitable for the Si IGBTs, but also available for the SiC devices. In the future, the SiC devices can be used to replace the Si IGBTs for the LLC resonant converter in the proposed configuration, which may further improve the efficiency and power density of PETT.

References

[1] A. Q. Huang, M. L. Crow, G. T. Heydt, J. P. Zheng and S. J. Dale, "The Future Renewable Electric Energy Delivery and Management (FREEDM) System: The Energy Internet," in *Proceedings of the IEEE*, vol. 99, no. 1, pp. 133-148, Jan. 2011.

[2] Z. Li, P. Wang, Z. Chu, H. Zhu, Z. Sun and Y. Li, "A three-phase 10 kVAC-750 VDC power electronic transformer for smart distribution grid," *2013 15th European Conference on Power Electronics and Applications (EPE)*, Lille, 2013, pp. 1-9.

[3] D. Wang, J. Tian, C, Mao, J. Lu, Y. Duan, J. Qiu, H. Cai, "A 10-kV/400-V 500-kVA Electronic Power Transformer," in *IEEE Transactions on Industrial Electronics*, vol. 63, no. 11, pp. 6653-6663, Nov. 2016.

[4] X. Yu, X. She, X. Zhou and A. Q. Huang, "Power Management for DC Microgrid Enabled by Solid-State Transformer," in *IEEE Transactions on Smart Grid*, vol. 5, no. 2, pp. 954-965, March 2014.

[5] B. Zhao, Q. Song, J. Li, W. Liu, G. Liu and Y. Zhao, "High-Frequency-Link DC Transformer Based on Switched Capacitor for Medium-Voltage DC Power Distribution Application," in *IEEE Transactions on Power Electronics*, vol. 31, no. 7, pp. 4766-4777, July 2016.

[6] C. Zhao, D. Dujic, A. Mester, J. K. Steinke, M. Weiss, S. L. Schmid, T. Chaudhuri and P. Stefanutti, "Power Electronic Traction Transformer—Medium Voltage Prototype," in *IEEE Transactions on Industrial Electronics*, vol. 61, no. 7, pp. 3257-3268, July 2014.

[7] D. Dujic, C. Zhao, A. Mester, J. K. Steinke, M. Weiss, S. L. Schmid, T. Chaudhuri and P. Stefanutti, "Power Electronic Traction Transformer-Low Voltage Prototype," in *IEEE Transactions on Power Electronics*, vol. 28, no. 12, pp. 5522-5534, Dec. 2013.

[8] J. Feng, W. Q. Chu, Z. Zhang and Z. Q. Zhu, "Power Electronic Transformer-Based Railway Traction Systems: Challenges and Opportunities," in *IEEE Journal of Emerging and Selected Topics in Power Electronics*, vol. 5, no. 3, pp. 1237-1253, Sept. 2017.

[9] Y. Lian, G. P. Adam, D. Holliday and S. J. Finney, "Medium-voltage DC/DC converter for offshore wind collection grid," in *IET Renewable Power Generation*, vol. 10, no. 5, pp. 651-660, May 2016.

[10] B. Sarlioglu and C. T. Morris, "More Electric Aircraft: Review, Challenges, and Opportunities for Commercial Transport Aircraft," in *IEEE Transactions on Transportation Electrification*, vol. 1, no. 1, pp. 54-64, June 2015.

[11] D. Bosich, A. Vicenzutti, R. Pelaschiar, R. Menis and G. Sulligoi, "Toward the future: The MVDC large ship research program," *2015 AEIT International Annual Conference (AEIT)*, Naples, 2015, pp. 1-6.

[12] J. E. Huber and J. W. Kolar, "Applicability of Solid-State Transformers in Today's and Future Distribution Grids," in *IEEE Transactions on Smart Grid*, to be published, doi: 10.1109/TSG.2017.2738610.

[13] J. Taufiq, "Power Electronics Technologies for Railway Vehicles," *2007 Power Conversion Conference - Nagoya*, Nagoya, 2007, pp. 1388-1393.

[14] M. Glinka, "Prototype of multiphase modular-multilevel-converter with 2 MW power rating and 17-level-output-voltage," *2004 IEEE 35th Annual Power Electronics Specialists Conference (IEEE Cat. No.04CH37551)*, 2004, pp. 2572-2576 Vol.4.

[15] N. Hugo, P. Stefanutti, M. Pellerin and A. Akdag, "Power electronics traction transformer," *2007 European Conference on Power Electronics and Applications*, Aalborg, 2007, pp. 1-10.

[16] M. Youssef, J. A. A. Qahouq and M. Orabi, "Analysis and design of LCC resonant inverter for the tranportation systems applications," *2010 Twenty-Fifth Annual IEEE Applied Power Electronics Conference and Exposition (APEC)*, Palm Springs, CA, 2010, pp. 1778-1784.

[17] C. Zhao, M. Weiss, A. Mester, S. L. Schmid, D. Dujic, J. K. Steinke and T. Chaudhuri, "Power electronic transformer (PET) converter: Design of a 1.2MW demonstrator for traction applications," *International Symposium on Power Electronics Power Electronics, Electrical Drives*, Automation and Motion, Sorrento, 2012, pp. 855-860.

[18] D. Dujic, G. K. Steinke, M. Bellini, M. Rahimo, L. Storasta and J. K. Steinke, "Characterization of 6.5 kV IGBTs for High-Power Medium-Frequency Soft-Switched Applications," in *IEEE Transactions on Power Electronics*, vol. 29, no. 2, pp. 906-919, Feb. 2014.

[19] T. Besselmann, A. Mester and D. Dujic, "Power Electronic Traction Transformer: Efficiency Improvements Under Light-Load Conditions," in *IEEE Transactions on Power Electronics*, vol. 29, no. 8, pp. 3971-3981, Aug. 2014.

[20] J. E. Huber and J. W. Kolar, "Optimum Number of Cascaded Cells for High-Power Medium-Voltage AC–DC Converters," in *IEEE Journal of Emerging and Selected Topics in Power Electronics*, vol. 5, no. 1, pp. 213-232, March 2017.

[21] C. Gu, Z. Zheng, L. Xu, K. Wang and Y. Li, "Modeling and Control of a Multiport Power Electronic Transformer (PET) for Electric Traction Applications," in *IEEE Transactions on Power Electronics*, vol. 31, no. 2, pp. 915-927, Feb. 2016.

[22] Z. Shu, Z. Kuang, S. Wang, X. Peng and X. He, "Diode-clamped three-level multi-module cascaded converter based power electronic traction transformer," *2015 IEEE 2nd International Future Energy Electronics Conference (IFEEC)*, Taipei, 2015, pp. 1-5.

[23] J. Liu, J. Zhang, T. Q. Zheng and J. Yang, "A Modified Gain Model and the Corresponding Design Method for an LLC Resonant Converter," in *IEEE Transactions on Power Electronics*, vol. 32, no. 9, pp. 6716-6727, Sept. 2017.

[24] Bing Lu, Wenduo Liu, Yan Liang, F. C. Lee and J. D. van Wyk, "Optimal design methodology for LLC resonant converter," *Twenty-First Annual IEEE Applied Power Electronics Conference and Exposition*, 2006. APEC '06, Dallas, TX, 2006, pp. 533-538.

[25] G. Ortiz, M. G. Leibl, J. E. Huber and J. W. Kolar, "Design and Experimental Testing of a Resonant DC–DC Converter for Solid-State Transformers," in *IEEE Transactions on Power Electronics*, vol. 32, no. 10, pp. 7534-7542, Oct. 2017.

[26] J. Zhang, J. Liu, J. Yang, N. Zhao, Y. Wang and T. Q. Zheng, "An LLC-LC Type Bidirectional Control Strategy for an LLC Resonant Converter in Power Electronic Traction Transformer," in *IEEE Transactions on Industrial Electronics*, vol. 65, no. 11, pp. 8595-8604, Nov. 2018.

[27] T. Guillod, J. E. Huber, G. Ortiz, A. De, C. M. Franck and J. W. Kolar, "Characterization of the voltage and electric field stresses in multi-cell solid-state transformers," *2014 IEEE Energy Conversion Congress and Exposition (ECCE)*, Pittsburgh, PA, 2014, pp. 4726-4734.

[28] W. Chen, X. Ruan, H. Yan and C. K. Tse, "DC/DC Conversion Systems Consisting of Multiple Converter Modules: Stability, Control, and Experimental Verifications," in *IEEE Transactions on Power Electronics*, vol. 24, no. 6, pp. 1463-1474, June 2009.

[29] Y. S. Lee and G. T. Cheng, "Quasi-Resonant Zero-Current-Switching Bidirectional Converter for Battery Equalization Applications," in *IEEE Transactions on Power Electronics*, vol. 21, no. 5, pp. 1213-1224, Sept.2006.

[30] Y. Shang, C. Zhang, N. Cui and J. M. Guerrero, "A Cell-to-Cell Battery Equalizer With Zero-Current Switching and Zero-Voltage Gap Based on Quasi-Resonant LC Converter and Boost Converter," in *IEEE Transactions on Power Electronics*, vol. 30, no. 7, pp. 3731-3747, July 2015.

[31] T. Zhao, G. Wang, S. Bhattacharya and A. Q. Huang, "Voltage and Power Balance Control for a Cascaded H-Bridge Converter-Based Solid-State Transformer," in *IEEE Transactions on Power Electronics*, vol. 28, no. 4, pp. 1523-1532, April 2013.

[32] J. Liu, J. Yang, J. Zhang, Z. Nan and Q. Zheng, "Voltage Balance Control Based on Dual Active Bridge DC/DC Converters in a Power Electronic Traction Transformer," in *IEEE Transactions on Power Electronics*, vol. 33, no. 2, pp. 1696-1714, Feb. 2018.

[33] W. Chen, X. Ruan, H. Yan and C. K. Tse, "DC/DC Conversion Systems Consisting of Multiple Converter Modules: Stability, Control, and Experimental Verifications," in *IEEE Transactions on Power Electronics*, vol. 24, no. 6, pp. 1463-1474, June 2009.

[34] D. Sha, Z. Guo, T. Luo and X. Liao, "A General Control Strategy for Input-Series–Output-Series Modular DC–DC Converters," in *IEEE Transactions on Power Electronics*, vol. 29, no. 7, pp. 3766-3775, July 2014.

[35] R. T. H. Li, M. Vancu, F. Canales and D. Aggeler, "High performance dc-dc converter for wide voltage range operation," *Proceedings of The 7th International Power Electronics and Motion Control Conference*, Harbin, 2012, pp. 1151-1158.

[36] J. Huber, G. Ortiz, F. Krismer, N. Widmer and J. W. Kolar, "η-ρ Pareto optimization of bidirectional half-cycle discontinuous-conduction-mode series-resonant DC/DC converter with fixed voltage transfer ratio," *2013 Twenty-Eighth Annual IEEE Applied Power Electronics Conference and Exposition (APEC)*, Long Beach, CA, 2013, pp. 1413-1420.

[37] Mouser Electronics. [Online]. Available: https://www.mouser.com/?utm_source=Baidu+Brandzone&utm_medium=cpc&utm_campaign=Brandzone+Main&utm_term=title.

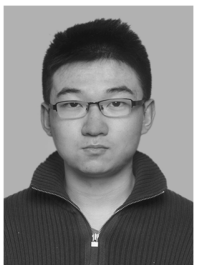

Jiepin Zhang (S'16) was born in Xinxiang, Henan, China, in 1991. He received the B.S. degree in electrical engineering from Beijing Jiaotong University, Beijing, China, in 2014, where he is now working for the Ph.D. degree in power electronics with the school of Electrical Engineering, Beijing Jiaotong University.

Presently, his research interests include dc/dc converters, stability of cascaded converters, traction drive system, and power electronic transformer.

This article has been accepted for publication in a future issue of this journal, but has not been fully edited. Content may change prior to final publication. Citation information: DOI 10.1109/TPEL.2018.2889107, IEEE Transactions on Power Electronics

Jianqiang Liu (M'13-SM'18) was born in Yangzhou, Jiangsu, China. He received the B.S. and Ph.D. degree in electrical engineering from Beijing Jiaotong University, Beijing, China, in 2003 and 2008, respectively.

Presently, he is an Associate Professor in the School of Electrical Engineering and a Research Scientist in the Institute of Power Electronics and Electric Traction, Beijing Jiaotong University. His research work is related to electric energy conversion, control of AC machines, and traction drive system.

Shigeng Zhong was born in Ruijin, Jiangxi Province, China, in 1995. He received the B.S. degree in electrical engineering from East China Jiaotong University, Nanchang, China in 2017. He is currently working toward the M.S. degree in power electronics with the school of Electrical Engineering, Beijing Jiaotong University.

His research interests include digital processing, auxiliary power supply, digital control, and power electronic transformer.

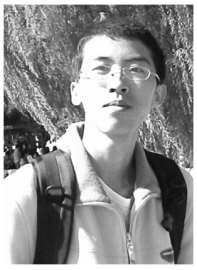

Jingxi Yang (S'16) was born in Shantou, Guangdong Province, China, in 1991. He received the B.S. degrees in electrical engineering from Beijing Jiaotong University, Beijing, China in 2014. He is currently working toward the Ph.D. degree in power electronics with the school of Electrical Engineering, Beijing Jiaotong University.

His research interests include modeling, digital control, multivariable control, and stability analysis in power electronic system, and power electronic transformer.

Nan Zhao (S'17) was born in Zhengzhou, Henan Province, China, in 1991. He received the B.S. degrees in electrical engineering from Beijing Jiaotong University, Beijing, China in 2014. He is currently working toward the Ph.D. degree in power electronics with the school of Electrical Engineering, Beijing Jiaotong University.

His research interests include digital processing, fault diagnosis and redundancy in traction drive system, and power electronic transformer.

Trillion Q. Zheng (Qionglin Zheng) (M'06-SM'07) was born in Jiangshan, Zhejiang Province, China, in 1964. He received the B.S. degree in electrical engineering from Southwest Jiaotong University, Sichuan, China in 1986 and the M.S. and Ph.D degrees in electrical engineering from Beijing Jiaotong University, China, in 1992 and 2002, respectively.

He is currently a University Distinguished Professor at Beijing Jiaotong University, China. He directs the Center for Electric Traction, founded by Ministry of Education, China. His research interests include power supply and AC Drive of railway traction systems, high performance and low loss for power electronics systems, PV based converters and control, and active power filter and power quality correction. He holds 17 china patents, and has published over 60 journal articles and more than 100 technical papers in conference proceedings.

From 2003 to 2011, he served as dean in the school of electrical engineering, at Beijing Jiaotong University. Now he is deputy director of council of Beijing Society for Power Electornics and a member of council of China Electrotechnical Society . He received the Excellent Teacher Award of Beijing Government (1997), Youth Award of Railway Science and Technology of Zhan Tianyou (2005). He was laureates of Youth Elite of Science and Technology of the Railway Ministry of China (1998) and of Zhongda Scholar for power electronics and motor drive area, by Delta Environmental and Educational Foundation (2007).